



HAL
open science

Is the boreal spring tropical Atlantic variability a precursor of the Equatorial Mode?

Marta Martín-Rey, Alban Lazar

► **To cite this version:**

Marta Martín-Rey, Alban Lazar. Is the boreal spring tropical Atlantic variability a precursor of the Equatorial Mode?. *Climate Dynamics*, 2019, 10.1007/s00382-019-04851-9 . hal-02171957

HAL Id: hal-02171957

<https://hal.science/hal-02171957>

Submitted on 3 Jul 2019

HAL is a multi-disciplinary open access archive for the deposit and dissemination of scientific research documents, whether they are published or not. The documents may come from teaching and research institutions in France or abroad, or from public or private research centers.

L'archive ouverte pluridisciplinaire **HAL**, est destinée au dépôt et à la diffusion de documents scientifiques de niveau recherche, publiés ou non, émanant des établissements d'enseignement et de recherche français ou étrangers, des laboratoires publics ou privés.

1 **Is the boreal spring tropical Atlantic variability**
2 **a precursor of the Equatorial Mode?**

3
4 Marta Martín-Rey ⁽¹⁻²⁾ and Alban Lazar ⁽¹⁾

5
6
7 (1) Laboratoire d’Oceanographie et du Climat: Expérimentation et Approches Numériques
8 (LOCEAN), Université Pierre et Marie Curie (UPMC), Universités Sorbonnes, Paris, France

9
10 (2) UMR5318 CECI CNRS-CERFACS, Toulouse, France

11
12 Corresponding author current address: Marta Martín del Rey. Departamento de
13 Oceanografía Física y Tecnológica, Instituto de Ciencias del Mar (ICM-CSIC), Passeig
14 Marítim de la Barceloneta, 37-49, 08003 Barcelona (Spain).

15
16 Email: mmartin@icm.csic.es; Phone number: +34 93 230 1145

17 ORCID number: 0000-0001-6234-0447

18
19
20 **Abstract**

21
22 The Equatorial Mode (EM) governs the tropical Atlantic inter-annual variability during
23 boreal summer. It has profound impacts on the climate of adjacent and remote areas.
24 However, predicting the EM is one of the most challenging and intriguing issues for the
25 scientific community. Recent studies have suggested a possible connection between the
26 boreal spring Meridional Mode (MM) and the EM through ocean wave propagation. Here,
27 we use a set of sensitivity experiments with a medium-resolution ocean model to
28 determine the precursor role of a MM to create equatorial SST variability. Our results
29 demonstrate that boreal summer equatorial SSTs following a MM, are subject to two
30 counteracting effects: the local wind forcing and remotely-excited oceanic waves. For a
31 positive MM, the anomalous easterly winds blowing along the equator, shallow the
32 thermocline, cooling the sea surface via vertical diffusion and meridional advection.
33 Anomalous wind curl excites a downwelling Rossby wave north of equator, which is
34 reflected at the western boundary becoming an equatorial Kelvin wave (KW). This
35 downwelling KW propagates eastward, deepening the thermocline and activating the
36 thermocline feedbacks responsible for the equatorial warming. Moreover, the local wind
37 forcing and RW-reflected mechanism have a significant and comparable impact on the
38 equatorial SST variability. Changes in the intensity and persistence of these distinct
39 forcings will determine the equatorial SST response during boreal summer. Our results
40 give a step forward to the improvement of the EM predictability.

41
42 **Key words:** tropical Atlantic, Meridional Mode, Equatorial Mode, ocean waves, SST
43 variability

46 **1. Introduction**

47

48 The Equatorial Mode (EM) or Atlantic Niño is an air-sea coupled mode that controls the
49 inter-annual tropical Atlantic variability during boreal summer (Zebiak 1993; Lübbecke
50 et al. 2018). During its positive phase, the EM is characterized by an anomalous warming
51 in the eastern equatorial Atlantic, accompanied by a reduction of the climatological trade
52 winds (Lübbecke et al. 2018). The EM is thought to be generated by ocean dynamics
53 (Keenlyside and Latif 2007; Lübbecke and McPhaden 2013; Polo et al. 2015a; Jouanno
54 et al. 2017; Martín-Rey et al. 2019), mainly driven by the Bjerknes feedback (Bjerknes
55 1969). The Bjerknes mechanism implies the propagation of oceanic waves as a response
56 of an anomalous wind burst in the western equatorial Atlantic (Keenlyside and Latif
57 2007). Indeed, several authors have underlined the potential role of oceanic waves in the
58 development and decay of the EM (Carton and Huang 1994; Polo et al. 2008a; Lübbecke
59 et al. 2010), shaping its distinct structure and timing (Martín-Rey et al. 2019). In recent
60 decades, additional mechanisms as air-sea fluxes (Nnamchi et al. 2015, 2016), equatorial
61 deep jets (Brandt et al. 2011) or meridional advection of subsurface temperature (Richter
62 et al. 2013) have been also proposed to generate the equatorial SST variability.

63

64 The EM has profound impacts on the climate of adjacent and remote areas. Fluctuations
65 in the onset and intensity of West African (Losada et al. 2012a; Rodríguez-Fonseca et al.
66 2015), Indian (Kucharski et al. 2008; 2009) and East-Asian Monsoon (Jin and Huo 2018)
67 have been found associated with the EM. Moreover, the EM influences the precipitation
68 regime over Europe and Mediterranean Sea (Losada et al. 2012b; Mohino and Losada
69 2015) and is able to favour the development of a next winter ENSO during certain decades
70 (Rodríguez-Fonseca et al. 2009; Martín-Rey et al. 2014; 2015; Polo et al. 2015b). Thus,
71 predicting the EM is one of the most challenging and intriguing issues for the scientific
72 community.

73

74 The EM emerges as an internal mode of tropical Atlantic variability, however, it is also
75 subject to multiple external forcings (Ruiz-Barradas et al. 2000; Czaja et al. 2002), which
76 provide additional sources for its predictability. In this sense, the North Atlantic
77 Oscillation and ENSO phenomenon are the main remote forcings (Latif and Grötzner
78 2000; Ruiz-Barradas et al. 2000; Handoh et al. 2006). Interestingly, within the tropical
79 Atlantic basin, a possible connection between the boreal spring Meridional Mode (MM)
80 and EM has been suggested (Servain et al. 1999; Murtugudde et al. 2001; Andreoli and
81 Kayano 2003; Foltz and McPhaden 2010a). The MM is characterized by an anomalous
82 inter-hemispheric SST gradient associated with anomalous winds blowing to the warmer
83 hemisphere (Nobre and Shukla 1996). Several mechanisms have been reported to explain
84 the interaction between these modes. Servain et al. (1999) stated that MM and EM can be
85 connected at decadal and short inter-annual time scales, via the latitudinal migration of
86 the Inter Tropical Convergence Zone (Murtugudde et al. 2001; Andreoli and Kayano
87 2003). The meridional advection of north tropical Atlantic subsurface temperature
88 anomalies (Richter et al. 2013) or the discharge of ocean heat content into the equatorial

89 wave guide (Huang and Shukla 1997; Zhu et al. 2012) could also link the tropical and
90 equatorial Atlantic variability.

91

92 Remarkably, a dynamical mechanism based on remotely-excited oceanic waves could
93 also mediate the MM-EM connection (Foltz and McPhaden 2010a). During the
94 development of the MM, an anomalous wind stress curl triggers a Rossby wave north of
95 the equator that propagates westward and is reflected at the western boundary. As a
96 consequence, it becomes a Kelvin wave that propagates along the equatorial wave guide,
97 impacting in the equatorial SST anomalies (Foltz and McPhaden 2010b; Burmeister et al.
98 2016). This wave-reflected mechanism has been considered as part of a destructive
99 interaction between the MM and EM (Foltz and McPhaden 2010a) or as responsible of
100 the inconsistent relationship between ENSO and EM (Lübbecke and McPhaden 2012).
101 However, recent studies highlight the potential role of the wave-reflected mechanism in
102 creating equatorial SST variability during boreal summer (Foltz and McPhaden 2010b;
103 Burmeister et al. 2016). Moreover, Martín-Rey et al. (2019) demonstrate that this ocean
104 wave propagation shapes the distinct structure and timing of the EM. Under this context,
105 disentangling the potential impact of the MM in the development of the Equatorial Mode
106 becomes necessary.

107

108 The present study aims to shed light about the precursor role of the MM to generate
109 equatorial Atlantic variability during the following summer. We will determine the
110 mechanisms associated with the development and decay of the MM, with a special focus
111 on the wave activity. Moreover, we will assess the relative contribution of the MM-
112 associated wind forcing and ocean wave propagation in the generation of equatorial SST
113 anomalies, and in turn, of an EM event. For this purpose, a set of sensitivity experiments
114 with the medium-resolution ocean NEMO model have been performed and analysed.

115

116 **2. Data and Methodology**

117

118 ***2.1 Observations model description***

119 To validate the ability of the model to reproduce the boreal spring tropical Atlantic
120 variability, observed SSTs are considered from the HadISST dataset (Rayner et al. 2003)
121 for the period 1960 to 2011.

122

123 The tropical Atlantic configuration of the ocean NEMO model (Madec 2008) has been
124 used (Faye et al. 2015). The horizontal resolution is $\frac{1}{4}^\circ$ with a tripolar grid and 46 z-
125 levels. The model is forced with observed meteorological atmospheric variables (air
126 temperature and air humidity at 2m, surface wind at 10m, shortwave and longwave
127 radiation and precipitation) from the DRAKKAR forcing sets, version DFS4.4 (Brodeau
128 et al. 2010). The air-sea fluxes and wind stress are computed interactively using the bulk
129 formula and providing them as outputs by NEMO model. In order to investigate the
130 mechanisms underlying the development of the MM and its potential connection to the
131 EM, a set of sensitivity experiments have been conducted:

132

- 133 • **INTER:** 52-year simulation forced with inter-annual air-sea fluxes for the period
134 1960-2011 (for more details, see Martín-Rey et al. (2019)).
135
- 136 • **MM-REF:** 1.5-year simulation forced with the composite air-sea fluxes
137 associated with a typical Meridional Mode event from July (year -1) to December
138 (year 0) (see Methods for more details). This simulation reproduces the growing
139 and decaying phase of the MM pattern, which allows us to assess the impact of
140 the MM in the following summer equatorial variability.
141
- 142 • **MM-WAVE:** 1.5-year simulation forced with the composite air-sea fluxes
143 associated with a typical Meridional Mode event from July (year -1) to June (year
144 0). This simulation is similar to MM-REF, but here the atmospheric forcings act
145 only until late spring and they are set to climatological values from July. MM-
146 WAVE allows for isolating the contribution of ocean wave propagation in the
147 generation of boreal summer equatorial SST anomalies.
148
- 149 • **MM-WIND:** 1.5-year simulation forced with the composite air-sea fluxes
150 associated with a typical Meridional Mode event from July (year 0) to December
151 (year 0). The atmospheric forcings have been set to climatological values from
152 July (year -1) to June (year 0). This simulation is similar to MM-REF, but here
153 the atmospheric forcings act only from late spring until winter months. Thus,
154 MM-WIND allows for isolating the role of the local wind forcing to create
155 equatorial SST anomalies during summer months.
156

157 The above-mentioned simulations start from the same initial conditions, taken from a
158 stabilized climatological run. The climatological simulation has been run for 10 years
159 using the climatological DFS4.4 forcings from the total period 1958-2011. For the MM-
160 WAVE and MM-WIND experiments, a smooth linear transition has been applied to the
161 atmospheric forcings during June, to minimize the initial shock of the model. Our
162 experimental design allows for determining the relative role played by the MM-associated
163 thermodynamic (surface wind) and dynamic processes (oceanic waves) in the
164 development of equatorial SST variability and, in turn, in the generation of a EM event,
165 during next summer.
166

167 The output variables used throughout the study are: SST, sea surface height (SSH), the
168 isotherm of 16°C as a proxy of the thermocline depth (D16), horizontal currents and wind
169 stress.
170

171 **2.2 Methods**

172
173 Seasonal anomalies have been computed by subtracting the seasonal cycle of the whole
174 period (1960-2011) for observations and INTER simulation. A high-pass 7-year cut-off
175 Butterworth filter (Butterworth 1930) has been applied to the anomalies to isolate the
176 inter-annual variability and remove the global warming trend.

177 The leading modes of boreal spring (March-April-May-June) SST variability have been
 178 computed using the Principal Component Analysis (PCA, Figure 1a-b). PCA decomposes
 179 the anomalous SST space-time field $Y(n_s, n_t)$ into a number of *modes of variability* that
 180 maximize its variance. Each mode of variability is formed by a spatial structure
 181 (Empirical Orthogonal Function, EOF) and a time series (Principal Component, PC),
 182 which explain a fraction of the total variance of the original SST field (von Storch and
 183 Zwiers 2001). A typical Meridional Mode has been constructed as a composite of 28
 184 events, defined as those years in which the MM time series exceeds ± 1 std over the whole
 185 period 1960-2011 (Figure 1c). The composite of its associated air-sea fluxes is used to
 186 force the sensitivity experiments described in Section 2.1.

187
 188 For the analysis of the MM-REF, MM-WAVE and MM-WIND experiments, the 5-day,
 189 monthly and seasonal anomalies are computed by subtracting the associated seasonal
 190 cycle from the climatological simulation. To better assess the wave activity, a band-pass
 191 Butterworth filter that retains the 60 days – 540 days frequency, has been applied to the
 192 5-day SSH, D16 and wind stress anomalies.

193
 194 Several climate indices have been defined to characterize the key regions of the MM and
 195 EM patterns. North Tropical Atlantic (NTA) index is referred to the averaged anomalous
 196 fields in the area $[50^\circ\text{W}-15^\circ\text{W}, 10^\circ\text{N}-20^\circ\text{N}]$, while the equatorial region is characterized
 197 by the Atl3 index $[20^\circ\text{W}-0^\circ, 3^\circ\text{N}-3^\circ\text{S}]$.

198
 199 The calculation of the Ekman velocity has been done according to the following formula:
 200

$$w_E = -curl(\tau/\rho f) = \partial(\tau_x/\rho f)/\partial y - \partial(\tau_y/\rho f)/\partial x$$

201
 202 where τ_x and τ_y are the zonal and meridional components of the wind stress, ρ is the sea
 203 water density and f is the Coriolis parameter.
 204

205 206 **2.3 Heat budget analysis**

207
 208 To explore the air-sea interactions responsible for the development and decay of the MM,
 209 a heat budget analysis has been carried out in the tropical Atlantic. Our model allows the
 210 interactive calculation of the heat budget in the mixed layer using the bulk formula. The
 211 different terms of equation [1] are provided as outputs by the model. The temporal
 212 variations of the mixed layer temperature are explained by the contribution of diverse
 213 terms (Peter et al. 2006; Martín-Rey et al. 2019):
 214

$$215 \partial_t \langle T \rangle = \underbrace{-\langle u \partial_x T \rangle - \langle v \partial_y T \rangle + \langle D_l(T) \rangle}_{a} - \underbrace{\frac{1}{h} \frac{\partial h}{\partial t} (\langle T \rangle - T_{z=-h}) - \langle w \partial_z T \rangle - \frac{1}{h} (\kappa_z \partial_z T)_{z=-h}}_{b} + \underbrace{\frac{Q_s(1-F_{z=-h}) + Q^*}{\rho_0 c_p h}}_{c} \quad [1]$$

216
 217
 218
 219

220 with $\langle * \rangle = \frac{1}{h} \int_{-h}^0 * dz$ where h is the depth of the mixed layer; T and T_h are the temperature
221 of the mixed layer and below the mixed layer respectively; u, v and w are the zonal,
222 meridional and vertical currents, respectively; D_l is the lateral diffusion operator and κ_z
223 is vertical mixing coefficient. Notice that the net surface heat fluxes, Q_{net} , is decomposed
224 into the non-solar (latent, sensible and longwave) Q^* and solar (shortwave) Q_s heat
225 fluxes. As not all the incident shortwave solar radiation will penetrate in the mixed layer,
226 the function $F_{z=-h}$ is included, which describes the fraction of shortwave fluxes absorbed
227 in this layer and thus contributing to the mixed layer heating. Finally, ρ_0 is the seawater
228 density and C_p is the seawater specific heat capacity coefficient.

229

230 The equation [1] shows that the tendency of the temperature in the mixed layer (left) can
231 be expressed as the sum of atmospheric and oceanic contributions. The atmospheric term
232 is referred to air-sea fluxes (c), while the oceanic component is associated with horizontal
233 terms (a, zonal and meridional advection and lateral diffusion) and vertical processes (b,
234 turbulent mixing, vertical advection and entrainment). This approach has been found to
235 be a very useful method to investigate the air-sea interactions involved in the tropical
236 Atlantic variability modes (Polo et al. 2015a; Martín-Rey et al. 2019).

237

238 **3. Results**

239

240 ***3.1 Tropical Atlantic inter-annual variability in boreal spring***

241

242 The Meridional Mode (MM) emerges as the second mode of tropical Atlantic SST
243 variability during boreal spring in both observations and INTER simulation for the period
244 1960-2011 (Figure 1a-b). It accounts for the 24.6% and 24.8% of the total variance in
245 observations and model simulation respectively. The inter-hemispheric SST gradient is
246 well captured by the model ($r = 0.96$), although the equatorial cooling displays a westward
247 extension reaching South American coast compared to the observations (Figure 1a-b).
248 This can be due to the equatorial cold bias of the model, associated with a thinner
249 equatorial mixed layer and reduced thermocline slope (Martín-Rey et al. 2019). The inter-
250 annual variability of the MM is also well reproduced by the INTER simulation over the
251 whole period ($r=0.9$, Figure 1c).

252

253 As a first attempt to evaluate the possible connection between MM and EM, lead-lag
254 correlation between the time series (PC2 fixed in MAMJ) of the MM and Atl3 SST index
255 from JFMA to DJFM has been computed (Figure 1d). Significant negative correlations
256 are found from previous winter to next summer, being maximum at lag 0 (MAMJ, up to
257 0.8). Our results show that the entire evolution of the MM is strongly linked to equatorial
258 SST anomalies. In particular, the correlation between MM and boreal summer (JJAS)
259 Atl3 index reaches 0.4-0.5, which suggests that the MM would explain around 20% of
260 the summer equatorial SST variability and thus an important contribution to the
261 generation of the EM (Figure 1d).

262

263 ***3.2 Air-sea interactions involved in the development of the MM***

264

265 To gain further understanding of the physical processes controlling the development of
266 the MM and its potential link to the EM, a sensitivity experiment based on a typical MM
267 pattern has been performed, hereinafter MM-REF (see section 2.2). This typical MM has
268 been computed as a composite MM SST pattern, which has a good agreement (not shown)
269 with the leading mode of boreal spring variability from INTER simulation (Figure 1b).
270 MM-REF reveals that the development of the MM starts in boreal winter (JFM) with a
271 reduction of the north-easterly trades, associated with an anomalous cyclonic circulation
272 (Figure 2a). These anomalous winds persist until late spring (Figure 2b), decreasing the
273 latent heat loss and warming the mixed layer (Figure 2d). In contrast, the trades intensify
274 in the south tropical Atlantic from boreal winter to spring (Figure 2a-b), enhancing the
275 evaporation and cooling the sea surface (not shown). Our results corroborate the role of
276 the air-sea fluxes to lead the large-scale structure of the MM, with a negligible
277 contribution of oceanic terms (Amaya et al. 2016; Chang et al. 1997, Wagner et al. 1996;
278 Carton et al. 1996).

279

280 This asymmetric SST structure causes a meridional sea surface pressure gradient (not
281 shown), according with the Wind-Evaporation-SST feedback (Amaya et al. 2016), given
282 rise to anomalous cross-equatorial winds blowing to the warmer hemisphere (Figure 2a-
283 c). Consequently, the easterlies are reinforced along the equator from winter to spring,
284 shallowing the thermocline and activating the ocean processes responsible for the surface
285 cooling (Figure 2a-c,e). During summer months, the MM-wind forcing decays and the
286 equatorial band warms up, due to vertical diffusion and meridional advection respectively
287 (Figure 2d-e). Notice that during the entire MM evolution, the air-sea fluxes tend to damp
288 the equatorial SST anomalies (blue line, Figure 2e). Thus, our results provide further
289 evidence of the essential role of ocean dynamics to control the equatorial SST variations
290 (Foltz et al. 2003; Peter et al. 2006; Polo et al. 2015a; Martín-Rey et al. 2019).

291

292 ***3.3 Wave propagation in the MM evolution***

293

294 During the development of the MM event, the atmospheric wind forcing originates an
295 anomalous zonal SSH gradient at the equator (shaded, Figure 3a). This east-west SSH
296 dipole shifts its phase during summer months (shaded, Figure 3b), resembling the Kelvin
297 and Rossby wave signature of the delayed oscillator mechanism (Suarez and Schopf
298 1988). This anomalous configuration suggests the existence of ocean wave activity during
299 the development and decay of the MM, according to previous findings (Foltz and
300 McPhaden 2010a; Burmeister et al. 2016). However, a better characterization of the ocean
301 wave propagation, as well as the mechanisms responsible of the excitation of Rossby and
302 Kelvin waves, is required.

303

304 Figure 3a reveals that an anomalous anticyclonic circulation produces a negative wind
305 stress curl north of the equator (purple vectors), causing an anomalous Ekman pumping
306 (positive Ekman velocity, black contours) and downwelling conditions around 30°W-

307 20°W from January to June (white box). This vertical Ekman velocity (dark grey line,
308 Figure 3c) is produced by an anomalous convergence of horizontal currents (purple line),
309 which causes the SSH to rise (orange line) and the thermocline to deepen from January
310 to May (magenta line, Figure 3c). The simultaneous alteration of off-equatorial surface
311 and subsurface suggests the excitation of a baroclinic ocean wave. To better visualize the
312 wave activity during the MM, time-longitude diagrams of filtered 5-day SSH anomalies
313 at 2°N-4°N and along the equator are displayed in Figure 4.

314

315 During the growing phase of the MM, an anomalous wind burst in the western equatorial
316 Atlantic [40°W-30°W], triggers a set of upwelling Kelvin waves, uKW1 and uKW2 (pink
317 arrows), propagating eastward from February to May and May to July respectively
318 (Figure 4b). The uKW1 and uKW2 resemble 2nd baroclinic modes (1.27 m/s and 1.45
319 m/s respectively; Illig et al. (2004); Polo et al. (2008b)) that shallow the thermocline and
320 favour the mixed layer cooling by vertical processes from February to July (Figure 2e).
321 Notice that uKW1 is reflected at the African coast, returning as an upwelling Rossby
322 wave (uRW1, ~ 0.59 m/s, 2nd baroclinic mode) along 2°N-4°N (pink arrow, Figure 4c).

323

324 During the decaying phase of the MM, a downwelling Rossby wave (dRW) is excited
325 north of the equator (Figure 4a), associated with an anomalous negative wind stress curl
326 (Figure 3c). The dRW propagates to the west as a 2nd baroclinic mode (~0.56 m/s) and is
327 reflected at the western boundary in June-July (Figure 4a), becoming an equatorial
328 downwelling Kelvin wave (dKW~1.4m/s, Figure 4b). From July to September, as the
329 dKW propagates eastward, the thermocline deepens setting up the favourable conditions
330 to warm the equator by vertical diffusion and meridional advection (Figure 2e).

331

332 Our results confirm the existence of RW-reflected mechanism during the MM evolution
333 proposed by previous studies (Foltz and McPhaden 2010a). Furthermore, we demonstrate
334 that oceanic waves modulate the development and decay of the Meridional Mode.
335 Locally-excited equatorial Kelvin waves contribute to generate the MM-associated
336 equatorial cold tongue, while remotely-excited Rossby wave tends to counteract these
337 equatorial SSTs during summer months. This is in agreement with Martín-Rey et al.
338 (2019) who suggested the crucial role of oceanic waves in shaping the distinct structure
339 and timing of the EM. Nevertheless, it is worth mentioning that we can interpret our
340 results as a two-way contribution of the MM to the equatorial SST anomalies during
341 boreal summer. On the one hand, local easterly winds produce a shallower equatorial
342 thermocline, favouring the surface cooling via vertical diffusion. On the other hand, the
343 north-equatorial wind curl triggers a downwelling RW boundary-reflected into a KW that
344 deepens the thermocline and sets up the favourable conditions to warm the equator. The
345 competition between both phenomena will determine the equatorial SST anomalies
346 during boreal summer, and thus, the potential relation between the MM and EM.

347

348 Under this context, a quantification of the relative contribution of the oceanic waves,
349 compared to the local wind forcing on the equatorial SST variability is necessary and will
350 be assessed in next section.

351

352 *3.4 Impact of the MM-associated ocean wave and wind forcing in the equatorial*
353 *Atlantic variability*

354

355 The boreal summer equatorial SST anomalies following the peak of the MM are subject
356 to two distinct contributions: the local wind forcing and the remotely-forced ocean waves.
357 To isolate the relative contribution of each forcing, two additional sensitivity experiments
358 have been performed, MM-WAVE and MM-WIND (for more details, see Section 2.2).
359 In the MM-WAVE, the atmospheric forcing is suppressed from June, allowing the free
360 propagation of the RW-reflected into the equatorial dKW (Figure 4) during summer
361 months. Complementary, MM-WIND experiment only considers the atmospheric forcing
362 from June, which allows for determining the impact of the local wind in the generation
363 of equatorial SST variability.

364

365 Figure 5 presents the summer (August) SST anomalies in the equatorial Atlantic for the
366 three sensitivity experiments. MM-WAVE and MM-WIND clearly illustrates a different
367 and opposite impact over the equatorial SSTs. While MM-WAVE shows a strong
368 equatorial warming in August (up to 0.5°C), MM-WIND presents a homogeneous surface
369 cooling (~ 0.2°-0.3°C). The temporal evolution of the 5-day SST and SSH anomalies in
370 the Atl3 region reveals that the equatorial band warms up two times faster in MM-WAVE
371 respect to MM-REF (0.165°C/month vs 0.062°C/month, Figure 5c), associated with the
372 early arrival of the dRW at the eastern equatorial Atlantic (thin pink line, Figure 5c).
373 Indeed, the dKW propagation is more than two time faster in absence of local wind (~3.4
374 m/s in MM-WAVE respect to 1.4 m/s in MM-REF). In MM-REF, the anomalous
375 easterlies blow against the wave propagation, establishing a competitive interaction
376 between both effects (thin purple line, Figure 5a). When the intensified equatorial winds
377 act alone during summer months, they are able to create an equatorial cooling up to 0.2°C
378 (orange line, Figure 5a).

379

380 This competition between the surface winds and ocean waves is clearly illustrated in the
381 heat budget analysis of the eastern equatorial Atlantic (Figure 6). In absence of wind
382 forcing, the propagation of the dKW deepen the thermocline, enhancing the contribution
383 of vertical processes (dark green line) responsible to warm the equator from July to mid-
384 August (dark blue line, Figure 6b). The horizontal terms has a negligible effect, while the
385 air-sea fluxes tend to damp the equatorial warming (light green and blue lines, Figure 6b).
386 In contrast, when both the atmospheric forcing is included, the positive temperature trend
387 exhibits large variations (dark blue line, Figure 6a) due to the dominant effect of
388 horizontal advection (light green line, Figure 6a) added to the air-sea fluxes (light blue
389 line, Figure 6c). Both phenomena tend to counteract the impact of the ocean dynamics
390 activated by the dKW propagation (dark green line, Figure 6a).

391

392 Our results bring to light the competition between two distinct forcings to create the
393 equatorial Atlantic variability during a MM event. Both, the MM-associated local surface
394 wind and remotely-excited oceanic waves control equatorial SST anomalies during next

395 summer. We have demonstrated for the first time that oceanic waves and wind forcing
396 have a significant and comparable impact in the generation of equatorial SST variability
397 (up to 0.2°C, Figure 5a), strong enough to generate an EM event during boreal summer.
398

399 It is worth-mentioning that our results are referred to a typical MM event in which the
400 local wind counteracts the ocean wave contribution, given rise to with quasi-neutral
401 equatorial SST conditions during boreal summer (Figure 2c and Figure 5a). However,
402 changes in the amplitude or persistence of the atmospheric and/or oceanic forcing could
403 modify the boreal summer equatorial SST response.
404

405 **4. Discussion and conclusions**

406
407 We have investigated the precursor role of the Meridional Mode in generating equatorial
408 Atlantic variability and potentially an Equatorial Mode event during next summer. For
409 this purpose, we have performed a set of sensitivity experiments with the ocean NEMO
410 model. The main conclusions achieved in the present study are:
411

- 412 • The model reproduces quite well the spatial structure and inter-annual variability
413 of the Meridional Mode (MM). The MM shows a strong connection with the
414 equatorial SST anomalies during its entire evolution.
415
- 416 • The inter-hemispheric SST gradient of the MM pattern is driven by
417 thermodynamic processes (air-sea fluxes), while equatorial SST anomalies are
418 controlled by ocean dynamics (vertical diffusion and horizontal advection).
419
- 420 • Oceanic waves contribute actively to the development and decay of the MM,
421 shaping the equatorial SST anomalies:
 - 422 ○ *During the growing phase of the MM:* anomalous wind burst in the
423 western equatorial Atlantic trigger a set of upwelling Kelvin waves (KW)
424 that propagate eastward during winter and spring, shallowing the
425 thermocline and favoring the equatorial cooling via vertical diffusion and
426 meridional advection.
427
 - 428 ○ *During the decaying phase of the MM:* an anomalous negative wind
429 stress curl north of the equator, originates an anomalous convergence of
430 surface currents and an Ekman pumping during boreal spring.
431 Consequently, the SSH elevates and the thermocline deepens, exciting a
432 downwelling Rossby wave that is reflected in the western boundary,
433 becoming an equatorial dKW in boreal summer. The dKW deepens the
434 thermocline, activating the vertical processes responsible to warm up the
435 equator.
436
437

438 ○ Two distinct forcings are responsible of the boreal summer equatorial
439 SSTs following a MM event: the local surface wind and the remotely-
440 excited oceanic waves. Both contributions show a significant and
441 comparable effect over the equatorial Atlantic SST variability. In
442 absence of local wind forcing, the equatorial band warms up two times
443 faster due to the early arrival of the dKW that activates the vertical
444 processes. However, the surface wind contribution shallows the
445 equatorial thermocline, favouring the surface cooling and counteracting
446 the oceanic wave effect.

447
448

449 In the present paper, we provide further evidence of the precursor role of the MM to
450 generate an EM during next summer. The equatorial SST variability is subject to two
451 distinct and competitive contributions that determine the equatorial SST response during
452 boreal summer. Remarkably, Figure 7 illustrates that there are some MM events followed
453 by the same-sign EM. The Meridional Mode event of 1966 was followed by a strong
454 equatorial warming, a positive Equatorial Mode-like pattern (Figure 7b-c). Similarly, for
455 the negative MM event of 2009 (Figure 7d-e). According to our results, during those MM
456 events, the reflected-RW mechanism was stronger than the local wind, being able to
457 transfer the north tropical SST anomalies to the equatorial band (Burmeister et al. 2016).
458 Thus, changes in the amplitude and strength of the MM-associated surface wind could
459 modulate the equatorial SSTs during next summer, and then the MM-EM connection.

460

461 Our results give a step forward in the better understanding of the processes controlling
462 the Meridional Mode and its connection to the equatorial Atlantic variability. Moreover,
463 this study provides evidence about the precursor role of the Meridional Mode to generate
464 an Equatorial Mode event during next summer, which could be very useful to improve
465 the predictability of the EM. Nevertheless, further research is still required to better
466 understand the interaction between the MM and EM, conciliating the distinct proposed
467 mechanisms as well as the possible multidecadal modulation by natural variability and
468 Global Warming.

469

470 **Acknowledgements:** The research leading to these results received funding from the EU
471 FP7/2007-2013 under Grant Agreement 603521 (PREFACE project), the MORDICUS
472 grant under contract ANR-13-SENV-0002-01, CNES/EUMETSAT (CNES - DIA/TEC-
473 2016.8595, EUM/LEO-JAS3/DOC/16/852054) and the MSCA-IF-EF-ST FESTIVAL
474 (H2020-EU project 797236). The observed SSTs from HadISST dataset were provided
475 by the MetOffice Hadley Centre, from its website
476 at <https://www.metoffice.gov.uk/hadobs/hadisst/>. The data from the INTER, MM-REF,
477 MM-WIND and MM-WAVE simulations are available from the authors upon request.

478 **Figure Caption**

479

480 **Figure 1. Observed and simulated Meridional Mode and its connection with**
481 **equatorial SST variability.** (a-b) Regression maps of the anomalous SSTs (in °C) on the
482 Principal Component (PC) of the second mode (EOF2) of inter-annual tropical Atlantic
483 variability in boreal spring (March-April-May-June) for the period 1960-2011 from
484 observations and INTER simulation. (c) Principal components of the observed (solid
485 orange line) and modelled (dashed pink line) Meridional Mode for the period 1960-2011.
486 Grey lines denote the ± 0.5 std threshold. (d) Lead-lag correlation between the 4-month
487 averaged SST anomalies in the Atl3 region [20°W-0°, 3°N-3°S] and the Meridional Mode
488 (PC2 of TA SST in MAMJ) for observations (pink dots) and INTER (green dots) during
489 the period 1960-2011. The PC2 of the Meridional Mode is fixed in MAMJ (Lag 0), thus,
490 negative lags (from JFMA to MAMJ) indicate Atl3 leading while positive lags (from
491 MAMJ to DJFM) imply the leadership of Meridional Mode over the equatorial SST
492 anomalies. Statistically significant scores at 95% confidence level according to a t-test
493 are shown in filled dots.

494

495 **Figure 2. Air-sea interactions underlying the development of the Meridional Mode.**
496 (a-c) Anomalous simulated SSTs (shaded, in °C) and observed surface wind forcing
497 (vectors, in m/s) from boreal winter (DJF), spring (MAM) and summer months (JJA) for
498 the MM-REF simulation. Composite surface winds used to force MM-REF come from
499 DFS4.4 dataset. (d-e) Temporal evolution of the heat budget terms in North Tropical
500 Atlantic, NTA [50°W-15°W, 5°N-20°N] and Atl3 [20°W-0°, 3°N-3°S] regions (green
501 boxes in (c)) from previous fall (year -1) to winter months (year 0) following the
502 Meridional Mode. The heat budget terms displayed are the tendency of the mixed layer
503 temperature (purple line), the air-sea fluxes (blue line) and oceanic horizontal (green line)
504 and vertical processes (red line). The data comes from MM-REF simulation.

505

506 **Figure 3. Excitation of ocean waves during the development of the Meridional Mode.**
507 (a-b) Anomalous temporal variations of SSH (shaded, in m), wind stress (purple vectors,
508 in N/m²) and vertical Ekman velocity (black contours, m/s) for boreal winter-spring
509 (January-May, a) and summer months (July-September, b) from MM-REF simulation.
510 (c) Seasonal evolution of monthly variations of SSH (solid orange line, in cm/day), D16
511 (solid pink line, in m), Ekman vertical velocity (solid black line, in m/day) and divergence
512 of the horizontal currents (solid purple line in m³/day) averaged [30°W-20°W, 3°N-6°N]
513 (white box in (a)). The monthly variations are computed as the difference between the
514 last 5-day mean data respect to the first 5-day mean data of each month.

515

516 **Figure 4. Equatorial wave propagation associated with the Meridional Mode.**
517 Time-longitude diagrams of anomalous filtered 5-days SSH anomalies (in cm) at 2°N-
518 4°N (a,c) and along the equator (b). Notice that the 2°N-4°N diagram has been duplicated
519 and the x-axis is reversed to better visualize the propagation and coastal-boundary
520 reflection of the Rossby and Kelvin waves along the equatorial Atlantic. The propagation

521 of Kelvin and Rossby waves are highlighted with white and pink arrows, for
522 downwelling and upwelling conditions respectively.

523

524 **Figure 5. Impact of the wave activity in the equatorial Atlantic variability.** (a-c)
525 Anomalous SST (shaded, in °C) and surface wind forcing (vector, in m/s) in the equatorial
526 Atlantic in August for MM-REF, MM-WAVE and MM-WIND. (d-e) Time series of
527 anomalous 5-day SST (solid thick lines, in °C) and SSH (solid thin lines, in cm) in the
528 Atl3 region for MM-REF, MM-WAVE and MM-WIND from January to December.

529

530 **Figure 6. Heat budget analysis in the eastern equatorial Atlantic.** (a-c) Anomalous 5-
531 day heat budget terms (temperature trend, air-sea fluxes, vertical and horizontal
532 processes, in °C/day) in MM-REF, MM-WAVE and MM-WIND simulations from
533 January to December.

534

535 **Figure 7. Meridional Mode followed by Equatorial Mode events.** (a) Time series of
536 Meridional Mode (PC2) and Equatorial Mode (Atl3) during 1960-2011 for observations
537 and INTER simulation. (b-e) Observed anomalous tropical Atlantic SSTs in boreal spring
538 (MAMJ) and summer (JJAS) months are displayed for two Meridional Mode events,
539 1966 and 2009. In both cases, pronounced equatorial SST anomalies during summer
540 months followed the development of a same-sign Meridional Mode event.

541

542

543

544

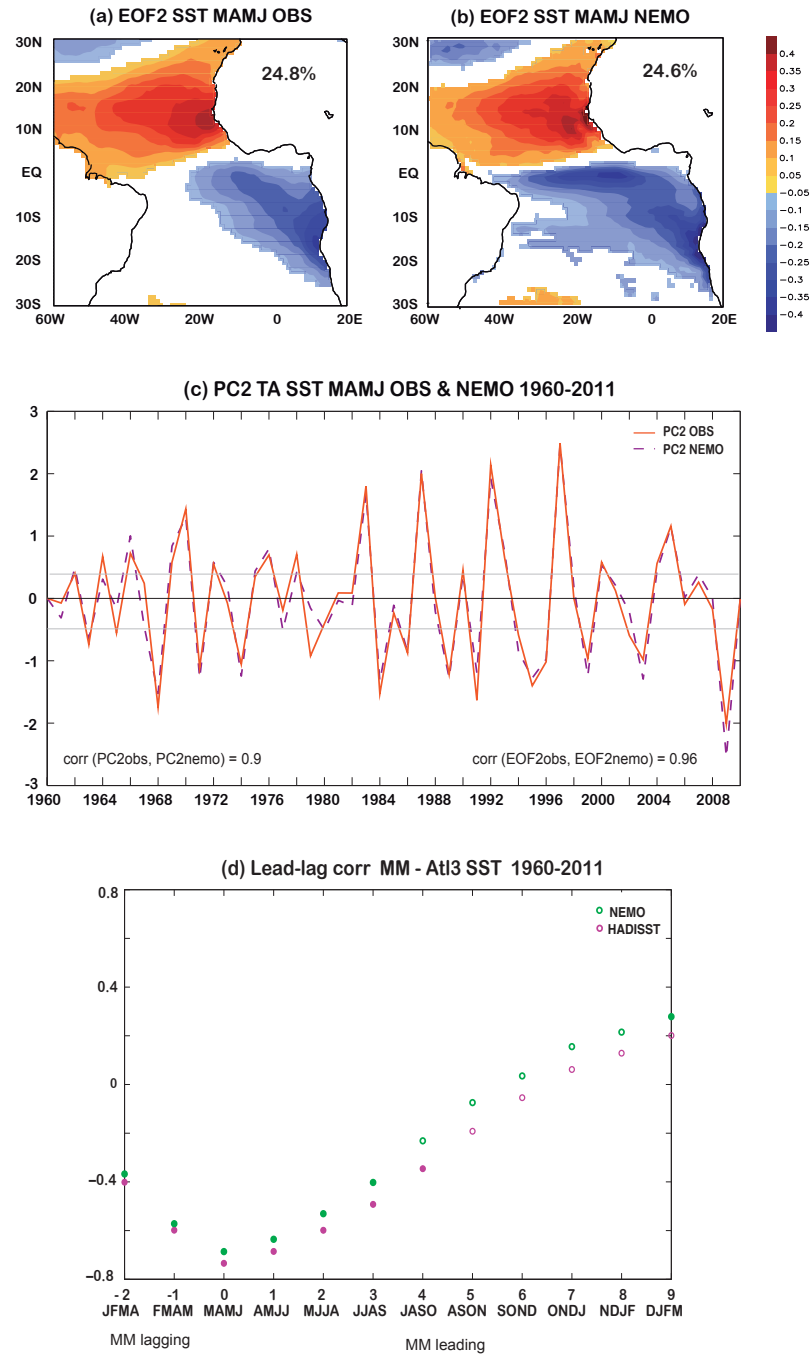


Figure 1. Observed and simulated Meridional Mode and its connection with equatorial SST variability. (a-b) Regression maps of the anomalous SSTs (in °C) on the Principal Component (PC) of the second mode (EOF2) of inter-annual tropical Atlantic variability in boreal spring (March-April-May-June) for the period 1960-2011 from observations and INTER simulation. (c) Principal components of the observed (solid orange line) and modelled (dashed pink line) Meridional Mode for the period 1960-2011. Grey lines denote the ± 0.5 std threshold. (d) Lead-lag correlation between the 4-month averaged SST anomalies in the Atl3 region [20°W-0°, 3°N-3°S] and the Meridional Mode (PC2 of TA SST in MAMJ) for observations (pink dots) and INTER (green dots) during the period 1960-2011. The PC2 of the Meridional Mode is fixed in MAMJ (Lag 0), thus, negative lags (from JFMA to MAMJ) indicate Atl3 leading while positive lags (from MAMJ to DJFM) imply the leadership of Meridional Mode over the equatorial SST anomalies. Statistically significant scores at 95% confidence level according to a t-test are shown in filled dots

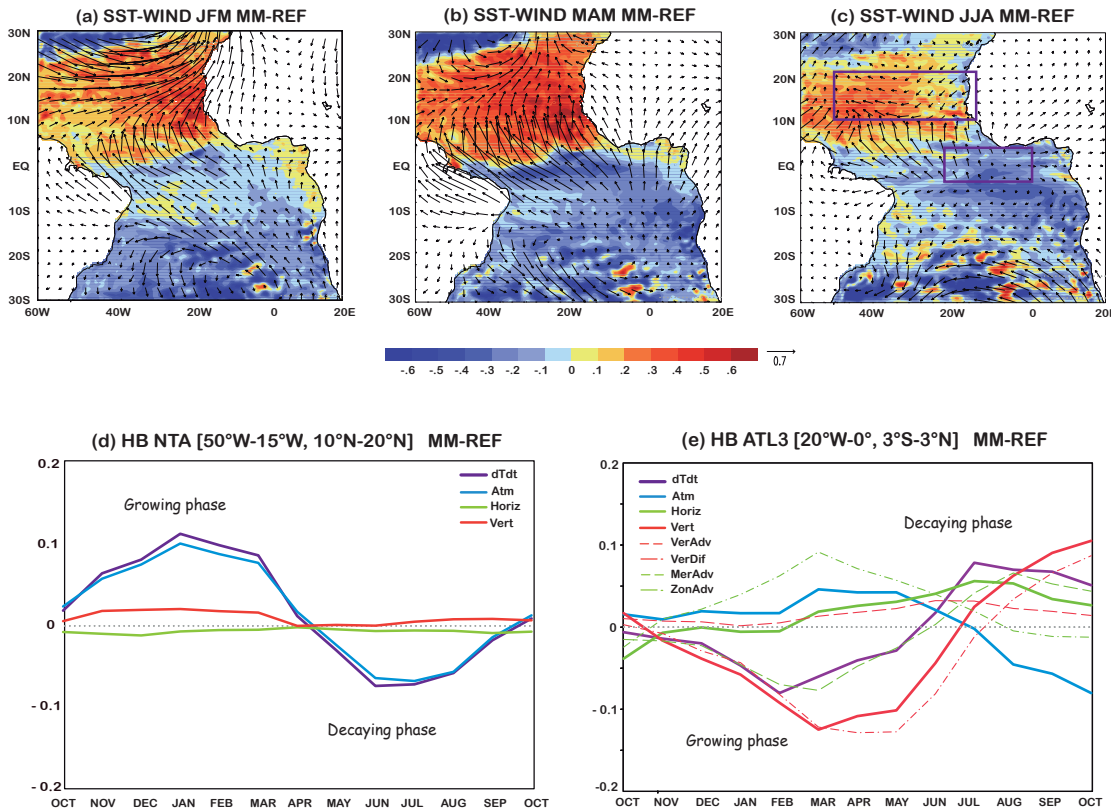


Figure 2. Air-sea interactions underlying the development of the Meridional Mode. (a-c) Anomalous simulated SSTs (shaded, in °C) and observed surface wind forcing (vectors, in m/s) from boreal winter (DJF), spring (MAM) and summer months (JJA) for the MM-REF simulation. Composite surface winds used to force MM-REF come from DFS4.4 dataset. (d-e) Temporal evolution of the heat budget terms in North Tropical Atlantic, NTA [50°W-15°W, 5°N-20°N] and AtI3 [20°W-0°, 3°N-3°S] regions (green boxes in (c)) from previous fall (year -1) to winter months (year 0) following the Meridional Mode. The heat budget terms displayed are the tendency of the mixed layer temperature (purple line), the air-sea fluxes (blue line) and oceanic horizontal (green line) and vertical processes (red line). The data comes from MM-REF simulation.

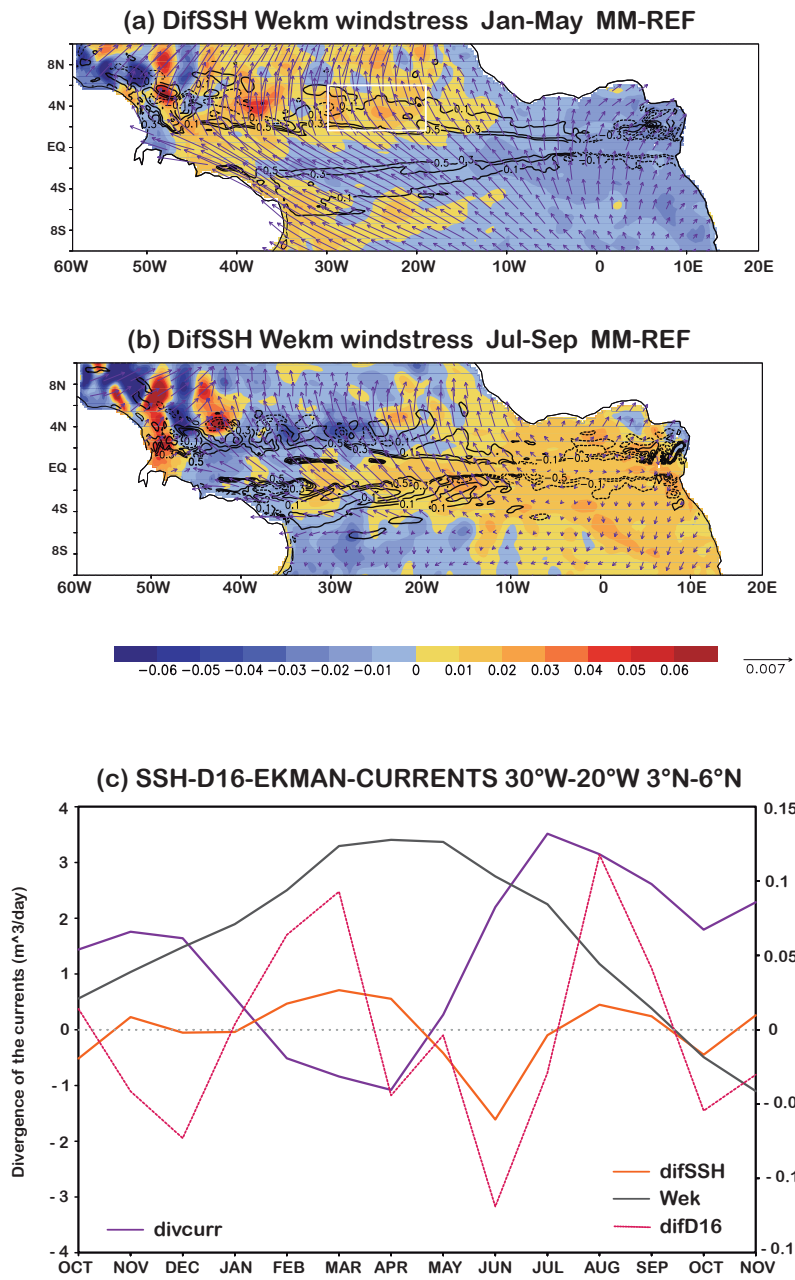


Figure 3. Excitation of ocean waves during the development of the Meridional Mode.

(a-b) Anomalous temporal variations of SSH (shaded, in m), wind stress (purple vectors, in N/m^2) and vertical Ekman velocity (black contours, m/s) for boreal winter-spring (January-May, a) and summer months (July-September, b) from MM-REF simulation. (c) Seasonal evolution of monthly variations of SSH (solid orange line, in cm/day), D16 (solid pink line, in m), Ekman vertical velocity (solid black line, in m/day) and divergence of the horizontal currents (solid purple line in m^3/day) averaged [$30^\circ W-20^\circ W$, $3^\circ N-6^\circ N$] (white box in (a)). The monthly variations are computed as the difference between the last 5-day mean data respect to the first 5-day mean data of each month

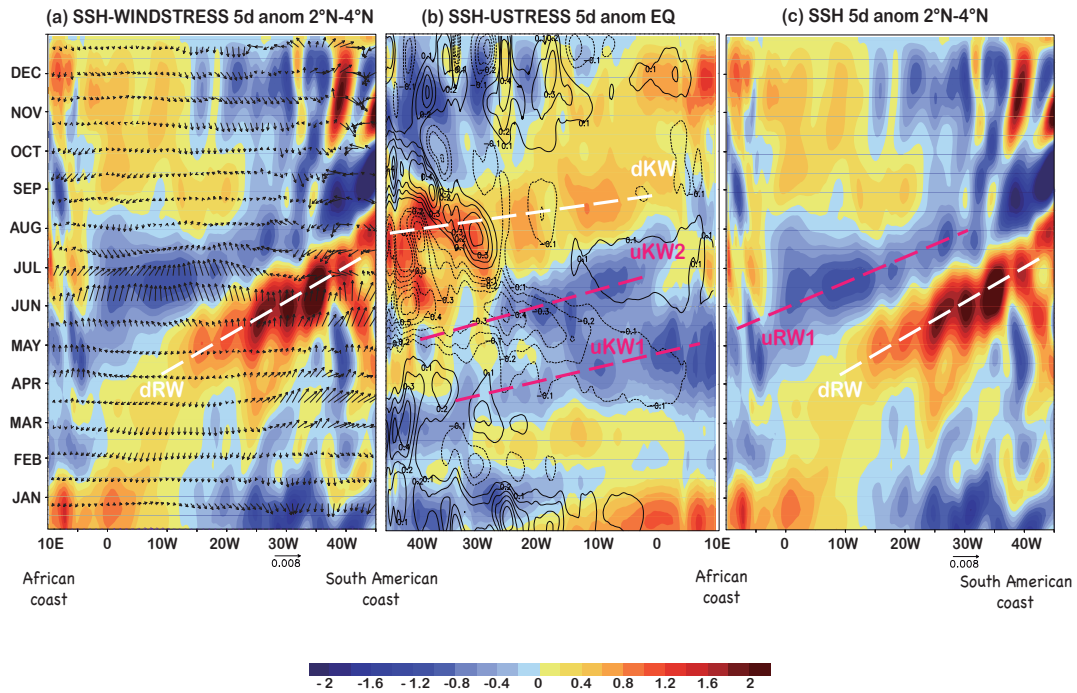


Figure 4. Equatorial wave propagation associated with the Meridional Mode.

Time-longitude diagrams of anomalous filtered 5-days SSH anomalies (in cm) at 2°N-4°N (a,c) and along the equator (b). Notice that the 2°N-4°N diagram has been duplicated and the x-axis is reversed to better visualize the propagation and coastal-boundary reflection of the Rossby and Kelvin waves along the equatorial Atlantic. The propagation of Kelvin and Rossby waves are highlighted with white and pink arrows, for downwelling and upwelling conditions respectively.

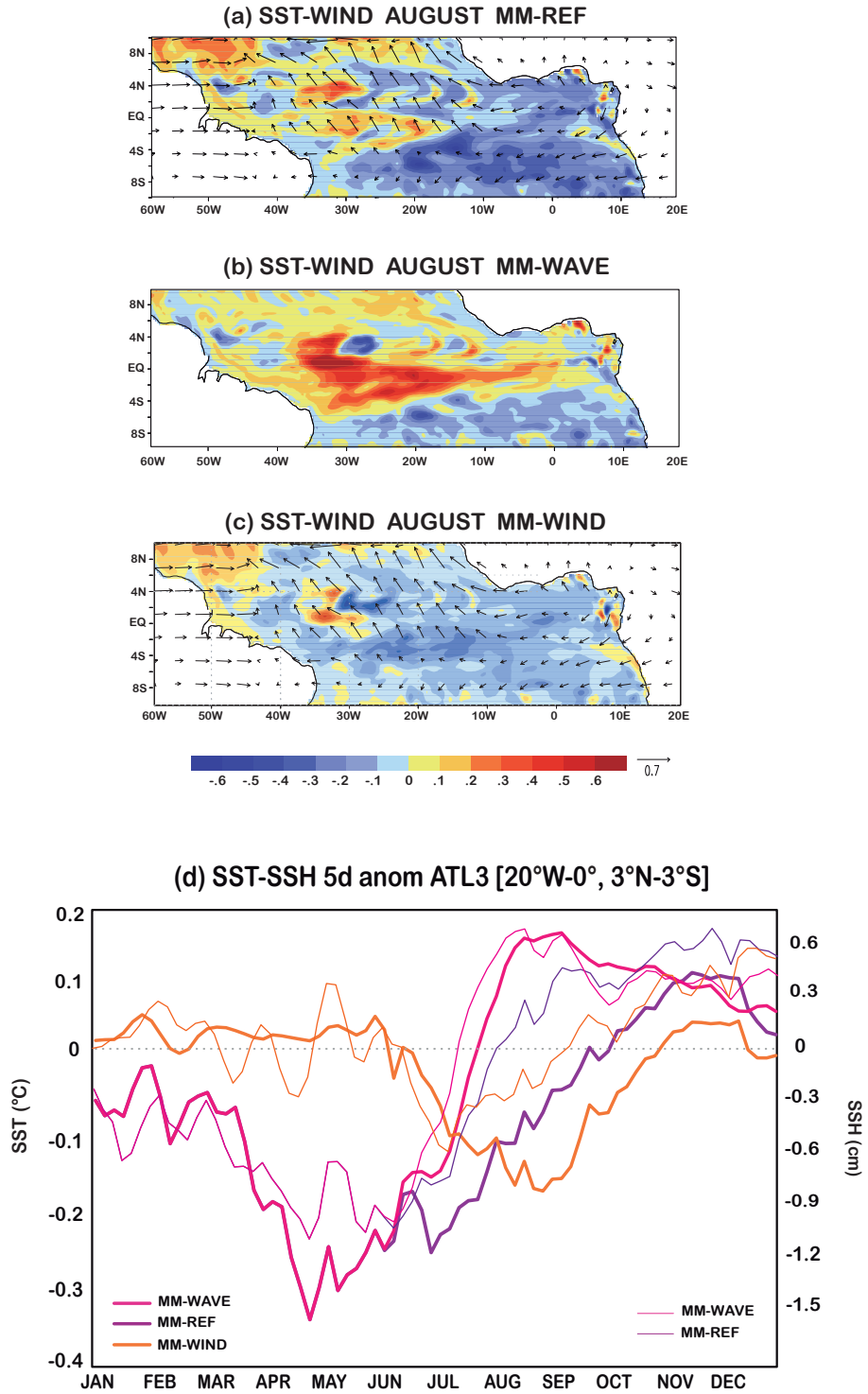


Figure 5. Impact of the wave activity in the equatorial Atlantic variability. (a-c) Anomalous SST (shaded, in °C) and surface wind forcing (vector, in m/s) in the equatorial Atlantic in August for MM-REF, MM-WAVE and MM-WIND. (d-e) Time series of anomalous 5-day SST (solid thick lines, in °C) and SSH (solid thin lines, in cm) in the Atl3 region for MM-REF, MM-WAVE and MM-WIND from January to December.

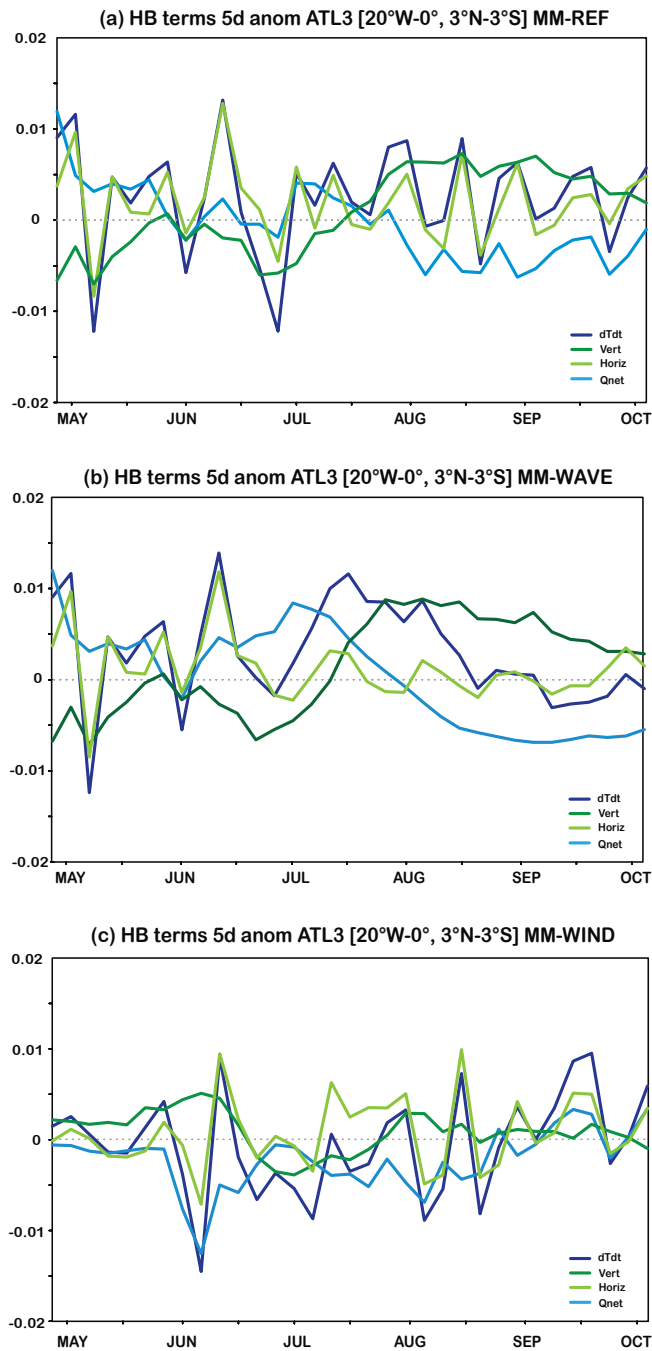


Figure 6. Heat budget analysis in the eastern equatorial Atlantic. (a-c) Anomalous 5-day heat budget terms (temperature trend, air-sea fluxes, vertical and horizontal processes, in °C/day) in MM-REF, MM-WAVE and MM-WIND simulations from January to December.

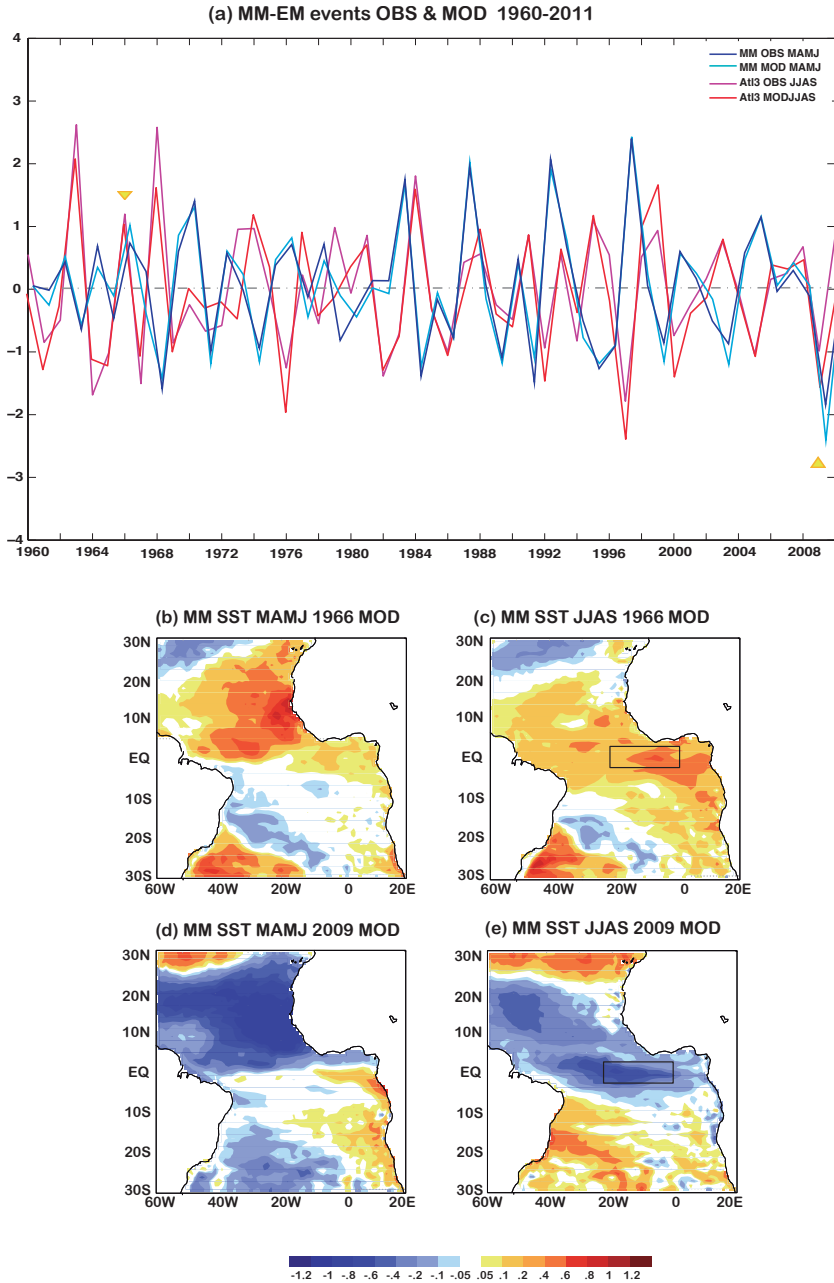


Figure 7. Meridional Mode followed by Equatorial Mode events. (a) Time series of Meridional Mode (PC2) and Equatorial Mode (Atl3) during 1960-2011 for observations and INTER simulation. (b-e) Observed anomalous tropical Atlantic SSTs in boreal spring (MAMJ) and summer (JJAS) months are displayed for two Meridional Mode events, 1966 and 2009. In both cases, pronounced equatorial SST anomalies during summer months followed the development of a same-sign Meridional Mode event.

References

- Amaya, D. J., M. J. DeFlorio, A. J. Miller, and S.-P. Xie, 2016: WES feedback and the Atlantic Meridional Mode: observations and CMIP5 comparisons. *Clim. Dyn.*, 1-15.
- Andreoli, R. V., and M. T. Kayano, 2003: Evolution of the equatorial and dipole modes of the sea-surface temperature in the Tropical Atlantic at decadal scale. *Meteorology and Atmospheric Physics*, **83**, 277-285.
- Bjerknes, J., 1969: Atmospheric teleconnections from the equatorial Pacific. *Mon. Wea. Rev.*, **97**, 163-172.
- Brandt, P., A. Funk, V. Hormann, M. Dengler, R. J. Greatbatch, and J. M. Toole, 2011: Interannual atmospheric variability forced by the deep equatorial Atlantic Ocean. *Nature*, **473**, 497.
- Brodeau, L., B. Barnier, A. M. Treguier, T. Penduff, and S. Gulev, 2010: An ERA40-based atmospheric forcing for global ocean circulation models. *Ocea. Mod.*, **31**, 88-104.
- Burmeister, K., P. Brandt, and J. Lübbecke, 2016: Revisiting the cause of the eastern equatorial Atlantic cold event in 2009. *J. Geophys. Res.: Oceans*, **121**, 4777-4789.
- Butterworth, S., 1930: On the theory of filter amplifiers. *Experimental wireless and the wireless engineer* **7**, 536-541.
- Carton, J. A., and B. Huang, 1994: Warm Events in the Tropical Atlantic. *J. Phys. Ocea.*, **24**, 888-903.
- Czaja, A., P. Van der Vaart, and J. Marshall, 2002: A Diagnostic Study of the Role of Remote Forcing in Tropical Atlantic Variability. *J. Climate*, **15**, 3280-3290.
- Faye, S., A. Lazar, B. Sow, and A. Gaye, 2015: A model study of the seasonality of sea surface temperature and circulation in the Atlantic North-eastern Tropical Upwelling System. *FrPhy*, **3**, 76.
- Foltz, G. R., and M. J. McPhaden, 2010a: Interaction between the Atlantic meridional and Niño modes. *Geophys. Res. Lett.*, **37**, L18604.
- , 2010b: Abrupt equatorial wave-induced cooling of the Atlantic cold tongue in 2009. *Geophys. Res. Lett.*, **37**, n/a-n/a.
- Foltz, G. R., S. A. Grodsky, J. A. Carton, and M. J. McPhaden, 2003: Seasonal mixed layer heat budget of the tropical Atlantic Ocean. *J. Geophys. Res.: Oceans*, **108**, 3146.
- Handoh, I. C., G. R. Bigg, A. J. Matthews, and D. P. Stevens, 2006: Interannual variability of the Tropical Atlantic independent of and associated with ENSO: Part II. The South Tropical Atlantic. *International Journal of Climatology*, **26**, 1957-1976.

- Huang, B., and J. Shukla, 1997: Characteristics of the Interannual and Decadal Variability in a General Circulation Model of the Tropical Atlantic Ocean. *J. Phys. Ocea.*, **27**, 1693-1712.
- Illig, S., and Coauthors, 2004: Interannual long equatorial waves in the tropical Atlantic from a high-resolution ocean general circulation model experiment in 1981–2000. *J. Geophys. Res.: Oceans*, **109**, n/a-n/a.
- Jin, D., and L. Huo, 2018: Influence of tropical Atlantic sea surface temperature anomalies on the East Asian summer monsoon. *Q.J.R. Met. Soc.*, **144**, 1490-1500.
- Jouanno, J., O. Hernandez, and E. Sanchez-Gomez, 2017: Equatorial Atlantic interannual variability and its relation to dynamic and thermodynamic processes. *Earth Systems Dynamics*, **8**, 1061-1069.
- Keenlyside, N. S., and M. Latif, 2007: Understanding Equatorial Atlantic Interannual Variability. *J. Climate*, **20**, 131-142.
- Kucharski, F., A. Bracco, J. H. Yoo, and F. Molteni, 2008: Atlantic forced component of the Indian monsoon interannual variability. *Geophys. Res. Lett.*, **35**, L04706.
- Kucharski, F., A. Bracco, J. H. Yoo, A. M. Tompkins, L. Feudale, P. Ruti, and A. Dell'Aquila, 2009: A Gill–Matsuno-type mechanism explains the tropical Atlantic influence on African and Indian monsoon rainfall. *Q.J.R. Met. Soc.*, **135**, 569-579.
- Latif, M., and A. Grötzner, 2000: The equatorial Atlantic oscillation and its response to ENSO. *Clim. Dyn.*, **16**, 213-218.
- Losada, T., B. Rodríguez-Fonseca, and F. Kucharski, 2012b: Tropical influence on the summer Mediterranean climate. *AtScL*, **13**, 36-42.
- Losada, T., B. Rodriguez-Fonseca, E. Mohino, J. Bader, S. Janicot, and C. R. Mechoso, 2012a: Tropical SST and Sahel rainfall: A non-stationary relationship. *Geophys. Res. Lett.*, **39**, L12705.
- Lübbecke, J., and M. J. McPhaden, 2012: On the Inconsistent Relationship between Pacific and Atlantic Niños*. *J. Climate*, **25**, 4294-4303.
- , 2013: A Comparative Stability Analysis of Atlantic and Pacific Niño Modes*. *J. Climate*, **26**, 5965-5980.
- Lübbecke, J., C. W. Böning, N. S. Keenlyside, and S.-P. Xie, 2010: On the connection between Benguela and equatorial Atlantic Niños and the role of the South Atlantic Anticyclone. *J. Geophys. Res.: Oceans*, **115**, C09015.
- Lübbecke, J., B. Rodríguez-Fonseca, I. Richter, M. Martín-Rey, T. Losada, I. Polo, and N. Keenlyside, 2018: Equatorial Atlantic variability - modes, mechanisms and global teleconnections. *Wiley Interdisciplinary Reviews: Climate Change*.
- Madec, G., 2008: NEMO ocean engine, Note du Pole de modélisation.

- Martín-Rey, M., B. Rodríguez-Fonseca, and I. Polo, 2015: Atlantic opportunities for ENSO prediction. *Geophys. Res. Lett.*, **42**, 6802-6810.
- Martín-Rey, M., B. Rodríguez-Fonseca, I. Polo, and F. Kucharski, 2014: On the Atlantic–Pacific Niños connection: a multidecadal modulated mode. *Clim. Dyn.*, **43**, 3163-3178.
- Martín-Rey, M., I. Polo, B. Rodríguez-Fonseca, A. Lazar, and T. Losada, 2019: Ocean dynamics shapes the structure and timing of tropical Atlantic variability modes *Geophys. Res. Lett.*, **submitted**.
- Mohino, E., and T. Losada, 2015: Impacts of the Atlantic Equatorial Mode in a warmer climate. *Clim. Dyn.*, **45**, 2255-2271.
- Murtugudde, R. G., J. Ballabrera-Poy, J. Beauchamp, and A. J. Busalacchi, 2001: Relationship between zonal and meridional modes in the tropical Atlantic. *Geophys. Res. Lett.*, **28**, 4463-4466.
- Nnamchi, H., J. Li, F. Kucharski, I.-S. Kang, N. S. Keenlyside, P. Chang, and R. Farneti, 2015: Thermodynamic controls of the Atlantic Niño. *Nature Communications*, **6**, 8895.
- , 2016: An Equatorial–Extratropical Dipole Structure of the Atlantic Niño. *J. Climate*, **29**, 7295-7311.
- Nobre, P., and J. Shukla, 1996: Variations in sea surface temperature, wind stress, and rainfall over the tropical Atlantic and South America. *J. Climate*, **9**, 2464-2479.
- Peter, A.-C., and Coauthors, 2006: A model study of the seasonal mixed layer heat budget in the equatorial Atlantic. *J. Geophys. Res.: Oceans*, **111**, C06014.
- Polo, I., B. Rodríguez-Fonseca, T. Losada, and J. García-Serrano, 2008a: Tropical Atlantic Variability Modes (1979–2002). Part I: Time-Evolving SST Modes Related to West African Rainfall. *J. Climate*, **21**, 6457-6475.
- Polo, I., A. Lazar, B. Rodríguez-Fonseca, and S. Arnault, 2008b: Oceanic Kelvin waves and tropical Atlantic intraseasonal variability: 1. Kelvin wave characterization. *J. Geophys. Res.: Oceans*, **113**, C07009.
- Polo, I., A. Lazar, B. Rodríguez-Fonseca, and J. Mignot, 2015a: Growth and decay of the equatorial Atlantic SST mode by means of closed heat budget in a coupled general circulation model. *Frontiers in Earth Science*, **3**, 37.
- Polo, I., M. Martín-Rey, B. Rodríguez-Fonseca, F. Kucharski, and C. Mechoso, 2015b: Processes in the Pacific La Niña onset triggered by the Atlantic Niño. *Clim. Dyn.*, **44**, 115-131.
- Rayner, N. A., and Coauthors, 2003: Global analyses of sea surface temperature, sea ice, and night marine air temperature since the late nineteenth century. *J. Geophys. Res.: Atmosphere*, **108**, 4407.

- Richter, I., S. K. Behera, Y. Masumoto, B. Taguchi, H. Sasaki, and T. Yamagata, 2013: Multiple causes of interannual sea surface temperature variability in the equatorial Atlantic Ocean. *Nature Geoscience*, **6**, 43-47.
- Rodríguez-Fonseca, B., I. Polo, J. García-Serrano, T. Losada, E. Mohino, C. R. Mechoso, and F. Kucharski, 2009: Are Atlantic Niños enhancing Pacific ENSO events in recent decades? *Geophys. Res. Lett.*, **36**, L20705.
- Rodríguez-Fonseca, B., and Coauthors, 2015: Variability and Predictability of West African Droughts: A Review on the Role of Sea Surface Temperature Anomalies. *J. Climate*, **28**, 4034-4060.
- Ruiz-Barradas, A., J. A. Carton, and S. Nigam, 2000: Structure of Interannual-to-Decadal Climate Variability in the Tropical Atlantic Sector. *J. Climate*, **13**, 3285-3297.
- Servain, J., I. Wainer, J. P. McCreary, and A. Dessier, 1999: Relationship between the equatorial and meridional modes of climatic variability in the tropical Atlantic. *Geophys. Res. Lett.*, **26**, 485-488.
- Suarez, M. J., and P. S. Schopf, 1988: A Delayed Action Oscillator for ENSO. *J. Atmos. Sci.*, **45**, 3283-3287.
- von Storch, H., and F. Zwiers, 2001: Statistical Analysis in Climate Research. *Cambridge University Press*, 484
- Zebiak, S. E., 1993: Air–Sea Interaction in the Equatorial Atlantic Region. *J. Climate*, **6**, 1567-1586.
- Zhu, J., B. Huang, and Z. Wu, 2012: The Role of Ocean Dynamics in the Interaction between the Atlantic Meridional and Equatorial Modes. *J. Climate*, **25**, 3583-3598.